Biological signal processing filters via engineering allosteric transcription factors

Thomas M. Groseclose[a], Ashley N. Hersey[a,1], Brian D. Huang[a,1], Matthew J. Realff[a], and Corey J. Wilson[a,2]

[a]School of Chemical and Biomolecular Engineering, Georgia Institute of Technology, Atlanta, Georgia 30332-2000

Edited by Stephen L. Mayo, California Institute of Technology, Pasadena, CA, and approved October 12, 2021 (received for review June 21, 2021)

Signal processing is critical to a myriad of biological phenomena (natural and engineered) that involve gene regulation. Biological signal processing can be achieved by way of allosteric transcription factors. In canonical regulatory systems (e.g., the lactose repressor), an INPUT signal results in the induction of a given transcription factor and objectively switches gene expression from an OFF state to an ON state. In such biological systems, to revert the gene expression back to the OFF state requires the aggressive dilution of the input signal, which can take 1 or more d to achieve in a typical biotic system. In this study, we present a class of engineered allosteric transcription factors capable of processing two-signal INPUTS, such that a sequence of INPUTS can rapidly transition gene expression between alternating OFF and ON states. Here, we present two fundamental biological signal processing filters, BANDPASS and BANDSTOP, that are regulated by D-fucose and isopropyl-β-D-1-thiogalactopyranoside. BANDPASS signal processing filters facilitate OFF–ON–OFF gene regulation. Whereas, BANDSTOP filters facilitate the antithetical gene regulation, ON–OFF–ON. Engineered signal processing filters can be directed to seven orthogonal promoters via adaptive modular DNA binding design. This collection of signal processing filters can be used in collaboration with our established transcriptional programming structure. Kinetic studies show that our collection of signal processing filters can switch between states of gene expression within a few minutes with minimal metabolic burden—representing a paradigm shift in general gene regulation.

synthetic biology | protein engineering | transcription factors | BANDPASS | BANDSTOP

Engineered gene circuits have become a hallmark of synthetic biology, a discipline which itself has come into fruition in recent years in pursuit of building robust and predictable parts and systems for biotechnological and biomedical applications (1–4). Synthetic genetic circuits have enabled the development of biological sensors (5) and switches (6), diagnostics and therapeutics (7, 8), and biological analogs to electrical and control devices and programs (9–17). Further advances in gene circuit design promise to facilitate increasingly complex methods to regulate biological processes (4, 18). Synthetic gene circuits have been routinely constructed via transcriptional regulation using allosteric transcription factors (TFs) (4, 6, 12, 13, 19). Allosteric TFs serve as simple genetic switches, whereby gene expression is modulated in response to environmental, cellular, and temporal signals (20, 21). Here, environmental signals (or INPUTS) interact with a TF's regulatory core domain (RCD), causing an allosteric shift in the protein's conformation to either increase or decrease the affinity of the TF's DNA-binding domain (DBD) for specific operator DNA sequences (21–23). Operators, DNA sequences specific to the DBD, are in proximity to gene promoters, thus allowing TFs to either inhibit transcription by compromising RNA polymerase (RNAP) binding (repressor) or facilitate transcription by recruiting RNAP (activator). Recent efforts have been made to expand the biological computing capacity of synthetic gene circuits administered by TFs through protein engineering. Domain swapping of one TF's RCD (responsive to a native ligand) with another's DBD (specific to a cognate operator) has been used to construct hybrid TFs with distinct and orthogonal DNA and ligand binding (12, 24–26). Novel protein chimeras have then been utilized in applications such as biological Boolean logic gates and biocontainment and biosecurity devices (12, 24, 25). The majority of allosteric TFs function as transcriptional repressors (X^+, where X denotes the TF RCD and therefore inducer ligand, and + denotes the repressor phenotype) (13, 21). Repressors are bound to DNA operators in the absence of the ligand, inhibiting transcription, and dissociate (are induced) when the ligand is present (21, 23). The engineering of the transcriptional antirepressor (X^A, where A indicates the antirepressor phenotype) has additionally resulted in increased computing capacity in synthetic biology (13, 27–30). While repressors function as Boolean BUFFER gates (12, 13), antirepressors function as Boolean NOT gates (13, 25, 30). That is to say, antirepressor-DNA affinity is increased when the ligand is present (anti-induced), inhibiting transcription.

Synthetic gene networks have been predominantly constructed using allosteric TFs with single cognate ligands (11–13). However, while some TFs have been demonstrated to be highly ligand specific (31, 32), even with regard to regioselectivity and stereoselectivity (33), others have been demonstrated to be promiscuous, typically for ligands with chemical similarity (34, 35). For instance, the lactose repressor (LacI)

Significance

As the size and complexity of genetic circuits increases, scientists and engineers need to find solutions to rapidly optimize flux and reduce the metabolic burden imposed on chassis cells. In this study, we report synthetic biology tools that imbue chassis cells with advanced signal processing functions akin to electrical devices commonly used in wireless transmitters and receivers (i.e., biological BANDPASS and BANDSTOP devices) that can simultaneously reduce metabolic burden. Moreover, this study presents a set of granular and more complete design rules for engineering allosteric transcription factors in the broader LacI/GalR topology. In addition, this study has improved our fundamental understanding of the plasticity and continuum of allosteric communication from the binding pocket to the protein–DNA interaction.

Author contributions: T.M.G., B.D.H., and C.J.W. designed research; T.M.G., A.N.H., and B.D.H. performed research; C.J.W. contributed new reagents/analytic tools; T.M.G., A.N.H., B.D.H., M.J.R., and C.J.W. analyzed data; and T.M.G. and C.J.W. wrote the paper.

The authors declare no competing interest.

This article is a PNAS Direct Submission.

[1]A.N.H. and B.D.H. contributed equally to this work.

[2]To whom correspondence may be addressed. Email: corey.wilson@chbe.gatech.edu.

This article contains supporting information online at http://www.pnas.org/lookup/suppl/doi:10.1073/pnas.2111450118/-/DCSupplemental.

Published November 12, 2021.

natively is induced by the lactose metabolic product allolactose but also responds to the gratuitous inducer isopropyl β-D-1-thiogalactopyranoside (IPTG) (35). In addition, for the LacI system, a variety of ligands (many of which are structurally similar galactopyranosides) have been shown to bind as 1) inducers, 2) anti-inducers (strengthening TF–DNA interactions), and 3) neutral (binding to the TF, but do not elicit a conformational change) (35, 36). The galactose isorepressor (GalS, S^+) is a transcriptional repressor that is responsible for regulating galactose carbon utilization in *Escherichia coli* (37, 38). As a constituent of the LacI/GalR family of TFs (21, 39), it bears high sequence conservation to LacI, likely possessing a DBD and ligand-responsive RCD—although no reported crystal structures exist for this TF. This predicted structural similarity has permitted the engineering of GalS:LacI chimeric TFs. Namely, the GalS RCD was equipped with the LacI wild-type YQR (corresponding to amino acid positions Y17, Q18, and R22) DBD, yielding the S^+_{YQR} TF, thereby allowing its regulation of the *lac* O^1 operator (12, 24, 39). Natively, GalS is induced by galactose, as well as exogenous, nonhydrolyzable D-fucose (37). Interestingly, IPTG prevents GalS from being induced (24, 40), even in the presence of saturating concentrations of D-fucose, likely due to competitive inhibition. IPTG and D-fucose vary by only two moieties on their hexose rings.

In this study, we successfully engineered a class of TFs via the GalS scaffold that interact with two distinct ligands, where one ligand elicits induction or anti-induction, and the other mitigates the processing of the initial INPUT signal. First, we engineered a D-fucose–responsive antirepressor beginning with the S_{YQR} scaffold. Akin to the repressor parent (S^+_{YQR}), the engineered antirepressor (S^A_{YQR}) was responsive to D-fucose (though antithetical [i.e., anti-induced]) and inhibited (mitigated anti-induction) by IPTG. Accordingly, we sought to evolve additional repressors and antirepressors in the GalS scaffold that respond functionally to IPTG. Namely, we successfully evolved a repressor and antirepressor in the GalS scaffold that responded to IPTG and were inhibited by D-fucose (i.e., inverted signal response). These multiple-ligand–responsive TFs function as integrated biological signal processing BANDPASS and BANDSTOP filters. Furthermore, following their adaptation with alternate DNA recognition (ADR) to create systems of orthogonal inducible promoters, we demonstrated their utility as open-loop controllers—providing the means to dynamically and simultaneously induce and anti-induce genes. This study represents an example of single TFs engineered with disparate functional and allosteric response toward two distinct ligands, in tandem with engineered alternate promoter recognition. These engineered TFs offer complex schema for gene regulation, granting the ability to control expression levels modulated by multiple input signals and, ultimately, a facile method to switch "OFF to ON to OFF" (BANDPASS) or "ON to OFF to ON" (BANDSTOP) genes in real time. Previous biological BANDPASS filters have required the use of complex networks of TFs (16, 17, 41). Likewise, previous examples of BANDSTOP equivalents used multilayered NOR gates via multiple chassis cells (42) or permanent genetic changes (15). Notably, earlier iterations of biological BANDPASS and BANDSTOP filters are significantly more complex and have markedly slower processing speeds relative to the devices presented in this study. Thus, our signal processing filters represent a paradigm shift in additive gene regulation (i.e., in terms of reduced complexity and increased speed). To our knowledge, this exists as a temporally controllable chemically inducible system with the aforementioned properties, with the only similar means for such gene regulation being optogenetics, with its own set of advantages and challenges (43).

Results

Constructing a BANDPASS Signal Processing Filter via the GalS Repressor. Previous studies have demonstrated that GalS (S^+_{YQR}) can be induced by the ligand D-fucose and antagonized by a noncognate ligand IPTG (24). Under saturating ligand conditions, induction of S^+_{YQR} by D-fucose can be regarded as a BUFFER logical operation, while the neutral binding of IPTG can be interpreted as a FALSE operation (i.e., IPTG can bind to the TF; however, the genetic circuit cannot be induced by the noncognate ligand) (Fig. 1*A* and *SI Appendix*, Fig. S1). In turn, the binding of the cognate ligand D-fucose to the repressor S^+_{YQR} can be evaluated in the context of dose–response (Fig. 1*B*). The resulting isotherm can be regarded as a transfer function, defined as the OUTPUT (green fluorescent protein [GFP]) as a function of the INPUT at steady state. Moreover, from a device perspective, the S^+_{YQR} TF when paired with a symmetric operator-promoter (S^+_{YQR} | O^{SYM}; *SI Appendix*, Fig. S1) the dose–response curve (as a function of D-fucose) can be regarded as a single INPUT transfer function, which can be represented as a HIGHPASS signal processing filter. Namely, the S^+_{YQR} (D-fucose) HIGHPASS signal processing filter is composed of a STOPBAND at low concentrations of D-fucose and a PASSBAND at high concentrations (>2.5 mM) of the cognate ligand (Fig. 1*B*). Pairing the PASSBAND state (i.e., at a fixed D-fucose concentration—10 mM) with progressive signal mitigation via the incremental increase of the IPTG signal, antagonized cognate ligand binding and reverted the unit operation back to the repressed (OFF) state (Fig. 1*C* and *SI Appendix*, Fig. S1*D*). As a unit operation, this system can be regarded as a BANDPASS signal processing device that can be turned ON via the signal D-fucose and subsequently turned OFF by way of the signal IPTG. Moreover, the placement of a given operator DNA element between the −35 and −10 hexamers of the promoter region reduces one aspect of metabolic burden on the chassis cell (44), illustrated in *SI Appendix*, Fig. S1*C* (also reference *SI Appendix*, Supplementary Note S1). Finally, we constructed a landscape composed of two transfer functions—D-fucose (*x*-axis, INPUT 1) and IPTG (*y*-axis, INPUT 2)—reporting the fraction of OUTPUT along the *z*-axis (Fig. 1*D*). Objectively, this two-INPUT system (device) represents a BANDPASS signal processing filter with a variable center. Each column after the transition (i.e., >2.5 mM D-fucose) can be regarded as a distinct PASSBAND. For a given PASSBAND, the progressive increase in IPTG correlated to the respective STOPBAND. In addition, the center of each BANDWIDTH shifted with an increase in D-fucose and required progressively higher concentrations of IPTG to mitigate induction—resulting in variable BANDWIDTH centers (*SI Appendix*, Supplementary Note S2). Similar performance was observed when the S^+_{YQR} TF was paired with a native nonsymmetric operator-promoter, forming the S^+_{YQR} | O^1 unit operation (*SI Appendix*, Fig. S1*E*).

Engineering Anti-GalS (S^A) TFs—A BANDSTOP Signal Processing Filter. Once we articulated the features of the initial S^+_{YQR} BANDPASS filter, our design goal was to engineer an antithetical TF—namely an anti-GalS (S^A_{YQR}) antirepressor. We posited that a S^A_{YQR} TF would represent the construction of a complementary signal processing device to the S^+_{YQR} BANDPASS (i.e., a S^A_{YQR} BANDSTOP that was responsive to the cognate ligand D-fucose and antagonized by IPTG) (Fig. 1*E* and *SI Appendix*, Fig. S2). To accomplish this, we leveraged the workflows that we developed in refs. 13 and 30, which required an initial block in allosteric communication (i.e., via conferred superrepression S^S_{YQR}) followed by one or more round(s) of error-prone PCR (EP-PCR). To identify putative superrepressor mutations, we performed a primary structure alignment

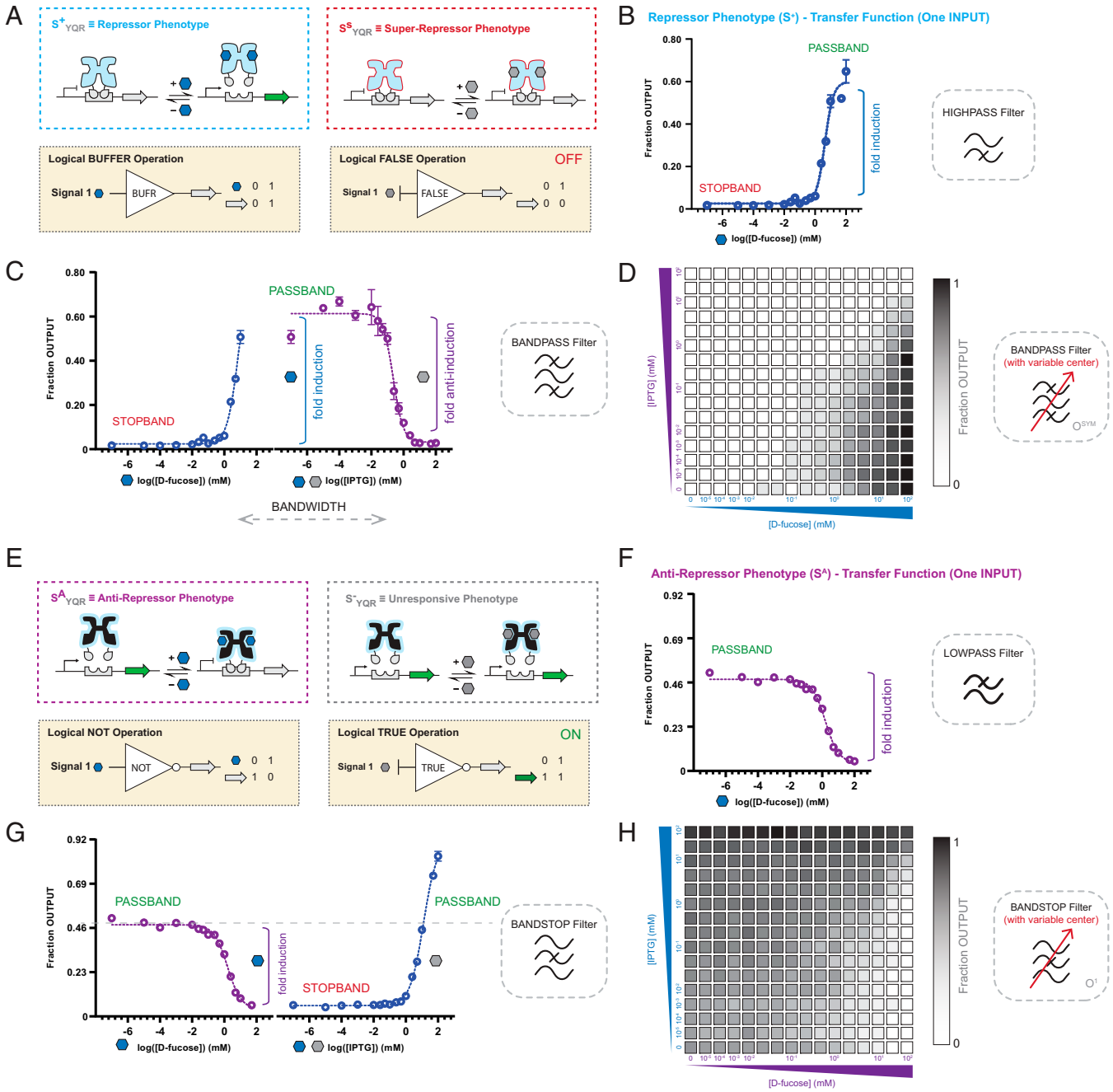

Fig. 1. S^{+}_{YQR} and S^{A}_{YQR} biological signal processing filters. (*A*) GalS (S^{+}_{YQR}) is induced by D-fucose, turning ON gene expression (repressor phenotype, blue), resulting in a BUFFER operation. S^{+}_{YQR} is not induced by IPTG, keeping gene expression OFF as a superrepressor (red) or a FALSE operation. (*B*) Transfer function for S^{+}_{YQR} | O^{SYM} with D-fucose. Increasing concentrations of D-fucose (*Bottom* axis, log scale) result in higher GFP fluorescence (Fraction OUTPUT, GFP fluorescence normalized to highest value observed) as a proxy for gene expression. This results in a HIGHPASS filter. (*C*) Addition of D-fucose induces S^{+}_{YQR}; however, addition of IPTG then causes mitigation of induction (blue curve, *Left*, to purple curve, *Right*), diminishing gene expression, resulting in a BANDPASS filter. (*D*) Heatmap of fluorescence OUTPUT for all combinations of D-fucose and IPTG with S^{+}_{YQR} | O^{SYM}, showing BANDPASS filters with variable centers. (*E*) Engineered anti-GalS (S^{A}_{YQR}) is anti-induced by D-fucose, turning OFF gene expression (antirepressor phenotype, purple), resulting in a NOT operation. S^{A}_{YQR} is not anti-induced by IPTG, keeping gene expression "ON" as an unresponsive phenotype (gray), or a TRUE operation. (*F*) Transfer function for S^{A}_{YQR} | O^{1} with D-fucose. Increasing concentrations of D-fucose (*Bottom* axis, log scale) result in lower GFP fluorescence (Fraction OUTPUT) as a proxy for gene expression. This results in a LOWPASS filter. (*G*) Addition of D-fucose anti-induces S^{A}_{YQR}; however, subsequent addition of IPTG then causes mitigation of anti-induction (purple curve, *Left*, to blue curve, *Right*), increasing gene expression, resulting in a BANDSTOP filter. (*H*) Heatmap of fluorescence OUTPUT for all combinations of D-fucose and IPTG with S^{A}_{YQR} | O^{1}, showing BANDSTOP filters with variable centers. In curves, circles show mean fluorescence (OD_{600} normalized) values of $n = 6$ biological replicates, with error bars representing ±1 SD. Dashed curves were fit using Hill functions. In heatmaps, each box represents mean normalized fluorescence of $n = 6$ measurements normalized to the highest and lowest fluorescence observed, from 0 (white) to 1 (black).

between LacI and GalS (*SI Appendix*, Fig. S3*A*). Here, we focused on positions 84, 95, and 96, as each of these positions have previously been used to confer superrepression in LacI, RbsR, and FruR (13) (i.e., TFs that share a topology with GalS). Initially, we started by performing saturation mutagenesis at each position—84, 95, and 96—using NNS (where N stands for any nucleotide and S stands for Cytosine or Guanine) codon degeneracy for an individual primary structure position. In this workflow, we used a microwell plate assay that we developed previously (12, 13), where GFP was the regulated reporter OUTPUT. Using the O^1 DNA operator—following our previously established workflows—we observed that at positions 84 and 95, multiple point mutations resulted in the superrepressor ($S^S{}_{YQR}$) phenotype (*SI Appendix*, Fig. S3 *B–D*). However, position 96 did not support superrepression. Moreover, antirepression was not conferred via a single point mutation—as in our previous study (13). Next, we pooled the five $S^S{}_{YQR}$ variants and performed a single round of EP-PCR (with a mutational rate of ∼2 to 5 per amplicon) to confer compensatory mutations and screened for antirepression (+/− D-fucose) using fluorescence-activated cell sorting (FACS) followed by validation using a microwell plate assay (*SI Appendix, Supplementary Methods*). After screening ∼10^8 cells, we identified a single anti-GalS variant that contained a L95A superrepressor mutation in addition to three compensatory mutations (S72T, L85Q, and M230L) (*SI Appendix*, Fig. S3*D*). The putative binding pocket for GalS is composed of positions L79, L160, N247, Y292, and M297 posited by Taylor et al. (45) and Wu et al. (34), in addition to an independent multiple sequence alignment. We surmised that none of the conferred mutations affected these positions or regions proximal to the putative ligand binding site or DNA binding site (*SI Appendix*, Fig. S4). Accordingly, we posited that antirepression was conferred by alternate allosteric communication—which is congruent with our previous reports (13, 29).

Next, we evaluated the D-fucose dose–response of the $S^A{}_{YQR}$ | O^1 unit operation (Fig. 1*E* and *SI Appendix*, Fig. S2). This experiment and analysis revealed that the $S^A{}_{YQR}$ | O^1 unit operation performed akin to a LOWPASS signal processing filter (i.e., as the concentration of the D-fucose INPUT ligand (signal) increased, the amount of GFP OUTPUT decreased) (Fig. 1*F*). Correspondingly, $S^A{}_{YQR}$ directed by the O^1 DNA operator was unresponsive to IPTG in the range of 0 to 0.1 mM INPUT. However, at higher concentrations of the antagonist, the $S^A{}_{YQR}$ TF was slightly induced (producing excess GFP) with a maximum dynamic range of 1.3 (*SI Appendix*, Fig. S2*B*). In turn, we evaluated whether the $S^A{}_{YQR}$ LOWPASS signal processing filter could be antagonized by IPTG—starting from a fixed signal concentration in the STOPBAND region. After bringing the system to a concentration of 10 mM D-fucose—resulting in a 12-fold anti-induction OFF state—we progressively added IPTG and evaluated cognate signal mitigation (Fig. 1*G*). Upon increasing the IPTG concentration to 2.5 mM, the anti-induced STOPBAND was reversed, recovering ∼100% of the original OUTPUT signal, collectively resulting in a $S^A{}_{YQR}$ BANDSTOP signal processing filter. In addition, increasing the IPTG concentration to values >2.5 mM resulted in a progressive increase in the production of the GFP OUTPUT (*SI Appendix*, Supplementary Note S3). Finally, we evaluated the $S^A{}_{YQR}$ BANDSTOP signal processing filter as a function of two INPUT variables—D-fucose and IPTG (Fig. 1*H*). Each row in the STOPBAND region (i.e., >1 mM D-fucose) defines the OFF state for a given BANDSTOP filter, and as the concentration of the cognate ligand increased, the center of the BANDWIDTH varied. Objectively, this can be regarded as a $S^A{}_{YQR}$ BANDSTOP signal processing filter with a variable center—that required increasing amounts of IPTG to recover the ON state, in proportion to the increase in the cognate ligand that facilitated the OFF state. In all cases, the ability to exceed the output dynamic range (post STOPBAND) was retained with sufficient concentrations of IPTG. Similar performance was observed when the $S^A{}_{YQR}$ TF was paired with a nonnative symmetric operator-promoter, forming the $S^A{}_{YQR}$ | O^{SYM} unit operation (*SI Appendix*, Fig. S2*E*).

Engineering a Signal Inverted BANDPASS Processing Filter. In our first device set, we presented two biological signal processing filters that were responsive to D-fucose and antagonized by IPTG—that is, a BANDPASS device and an engineered BANDSTOP device (Fig. 1). Given that GalS ($S^+{}_{YQR}$ and $S^A{}_{YQR}$) can interact neutrally with IPTG, we posited that the GalS regulatory core could be engineered to respond to IPTG. To test this hypothesis, we rescreened our original library (i.e., generated via EP-PCR)—however, in this iteration we screened for mutated GalS TFs that could be induced or anti-induced by IPTG. To facilitate the discovery of IPTG-responsive TFs derived from a mutated GalS primary scaffold, we used FACS, followed by a microwell plate assay validation in which we searched for phenotypes that increased or reduced the expression of GFP upon the addition of IPTG. We identified three variants that were responsive to IPTG as antirepressors and one variant that was responsive to IPTG as a repressor. Next, we evaluated each of the engineered TFs for sensitivity to D-fucose as a sole INPUT. Only one TF did not have an appreciable response to D-fucose in the range tested, while presenting sensitivity to the IPTG ligand, we designated this variant as $_SI^+{}_{YQR}$ (Fig. 2 and *SI Appendix*, Fig. S5 *A* and *B*). The $_SI^+{}_{YQR}$ variant only required one compensatory mutation (S72T) (*SI Appendix*, Fig. S3*D*).

Given that the $_SI^+{}_{YQR}$ TF could be induced by IPTG and was neutral to D-fucose (Fig. 2*A* and *SI Appendix*, Fig. S5 *A* and *B*), we surmised that the noncognate ligand (D-fucose) could potentially antagonize $_SI^+{}_{YQR}$ preinduced by IPTG. To test this assertion, first we evaluated the dose–response of the $_SI^+{}_{YQR}$ | O^1 unit operation with the cognate ligand IPTG (Fig. 2*B*). The resulting single INPUT transfer function objectively represents a HIGHPASS signal processing filter—with a STOPBAND between 0 and 0.5 mM IPTG and a PASSBAND > 0.5 mM IPTG. In turn, we tested for signal-induced mitigation of the $_SI^+{}_{YQR}$ | O^1 unit operation with a PASSBAND fixed at 5 mM IPTG, via the progressive addition of D-fucose (Fig. 2*C*). Increasing the D-fucose signal to 100 mM resulted in a 100% rejection (reduction) of the OUTPUT signal. Objectively, the $_SI^+{}_{YQR}$ BANDPASS device presented in Fig. 2*C* functioned via an inverted signal processing of IPTG and D-fucose—relative to the $S^+{}_{YQR}$ BANDPASS presented in Fig. 1*C*. This result is in contrast to wild-type LacI ($I^+{}_{YQR}$), which is induced by the cognate ligand; however, was not antagonized by D-fucose (*SI Appendix*, Fig. S6). Moreover, the addition of IPTG and D-fucose simultaneously to the wild-type LacI unit operation did not result in an apparent competition. Finally, we evaluated the performance of the $_SI^+{}_{YQR}$ BANDPASS as a function of two variables (i.e., IPTG and D-fucose) (Fig. 2*D*). Congruent with the $S^+{}_{YQR}$ BANDPASS, the $_SI^+{}_{YQR}$ BANDPASS device displayed a variable BANDWIDTH center—though signal inverted. In other words, as the concentration of IPTG increased in the PASSBAND region, a corresponding increase in the concentration of D-fucose was required to return the system to the OFF state. Interestingly, under low-concentration PASSBAND conditions (<5 mM IPTG), the addition of excess D-fucose (100 mM) resulted in superanti-induction (i.e., reduced leakiness relative to the no ligand condition with a maximum dynamic range of ∼2.0). Similar performance was observed when the $_SI^+{}_{YQR}$ TF was paired with a nonnative symmetric operator-promoter, forming the $_SI^+{}_{YQR}$ | O^{SYM} unit operation (*SI Appendix*, Fig. S5*E*).

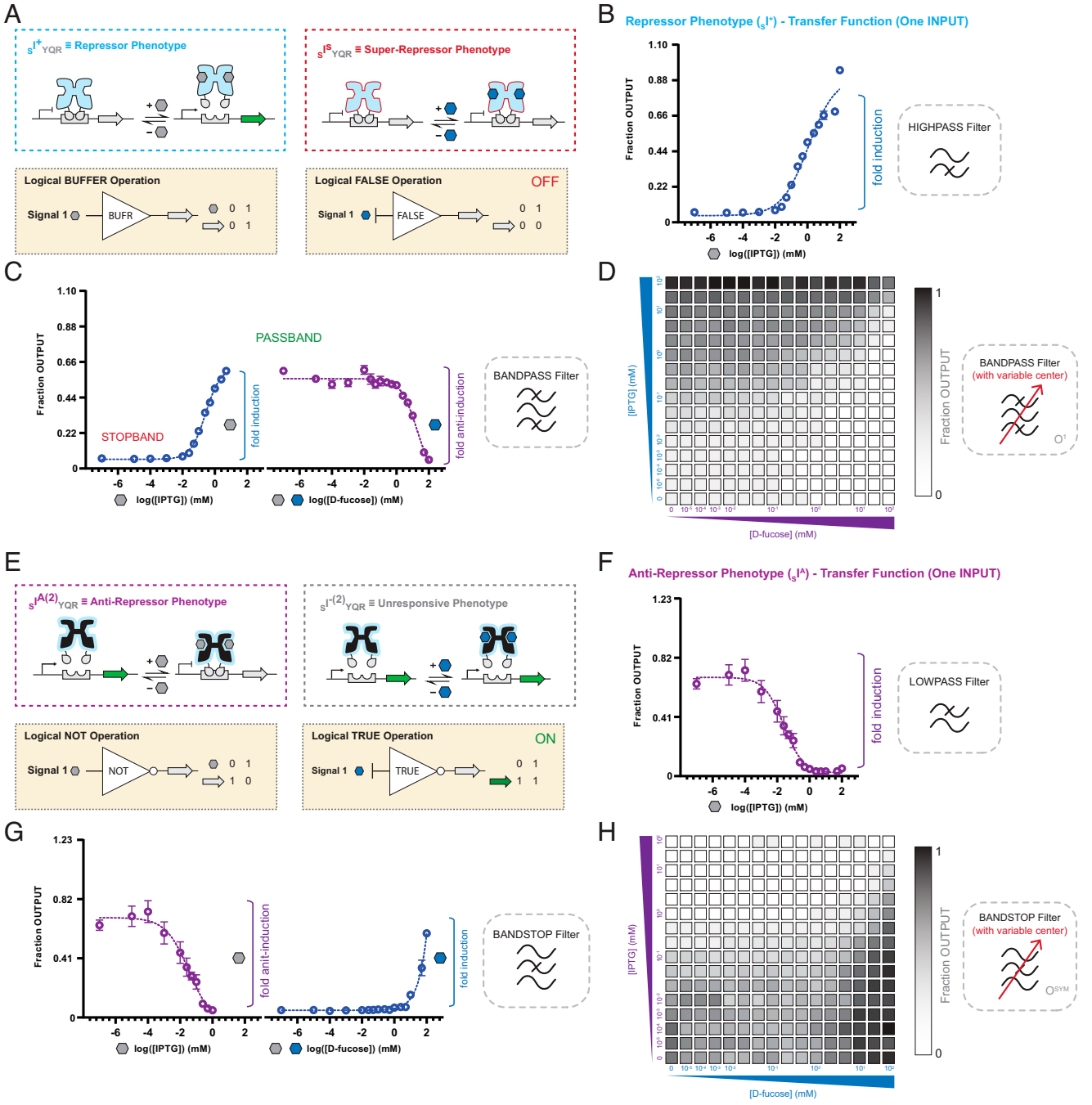

Fig. 2. $_{s}I^{+}{}_{YQR}$ and $_{s}I^{A(2)}{}_{YQR}$ biological signal processing filters. (*A*) Engineered IPTG-responsive GalS repressor ($_{s}I^{+}{}_{YQR}$) is induced by IPTG, turning ON gene expression (repressor phenotype, blue), resulting in a BUFFER operation. $_{s}I^{+}{}_{YQR}$ is not induced by D-fucose, keeping gene expression OFF as a superrepressor phenotype (red), or a FALSE operation. (*B*) Transfer function for $_{s}I^{+}{}_{YQR}$ | O^{1} with IPTG. Increasing concentrations of IPTG (*Bottom* axis, log scale) result in higher GFP fluorescence (Fraction OUTPUT, GFP fluorescence normalized to highest value observed) as a proxy for gene expression. This results in a HIGHPASS filter. (*C*) Addition of IPTG induces $_{s}I^{+}{}_{YQR}$ | O^{1}; however, addition of D-fucose then causes mitigation of induction (blue curve, *Left*, to purple curve, *Right*), diminishing gene expression, resulting in a BANDPASS filter. (*D*) Heatmap of fluorescence OUTPUT for all combinations of IPTG and D-fucose with $_{s}I^{+}{}_{YQR}$ | O^{1}, showing BANDPASS filters with variable centers. (*E*) Engineered IPTG-responsive GalS antirepressor ($_{s}I^{A(2)}{}_{YQR}$) is anti-induced by IPTG, turning OFF gene expression (antirepressor phenotype, purple), resulting in a NOT operation. $_{s}I^{A(2)}{}_{YQR}$ is not anti-induced by D-fucose, keeping gene expression ON as an unresponsive phenotype (gray), or a TRUE operation. (*F*) Transfer function for $_{s}I^{A(2)}{}_{YQR}$ | O^{sym} with IPTG. Increasing concentrations of IPTG (*Bottom* axis, log scale) result in lower GFP fluorescence (Fraction OUTPUT) as a proxy for gene expression. This results in a LOWPASS filter. (*G*) Addition of IPTG anti-induces $_{s}I^{A(2)}{}_{YQR}$; however, subsequent addition of D-fucose then causes mitigation of anti-induction (purple curve, *Left*, to blue curve, *Right*), increasing gene expression, resulting in a BANDSTOP filter. (*H*) Heatmap of fluorescence OUTPUT for all combinations of IPTG and D-fucose with $_{s}I^{A(2)}{}_{YQR}$ | O^{sym}, showing BANDSTOP filters with variable centers. In curves, circles show mean fluorescence values (OD_{600} normalized) of $n = 6$ biological replicates, with error bars representing ±1 SD. Dashed curves were fit using Hill functions. In heatmaps, each box represents mean normalized fluorescence of $n = 6$ measurements normalized to the highest and lowest fluorescence observed, from 0 (white) to 1 (black).

Engineering a Signal Inverted BANDSTOP Filter. In our initial search, we identified two variants that were responsive to IPTG—while either being nonresponsive or inversely responsive to D-fucose (*SI Appendix*, Figs. S3, S5, and S7). The first variant ${}_{S}I^{+}{}_{YQR}$ BANDPASS displayed a repressive phenotype to IPTG and neutral response to D-fucose, discussed in *Engineering a Signal Inverted BANDPASS Processing Filter*. In contrast, the other variant (${}_{S}I^{A(2)}{}_{YQR}$) presented an antirepressive phenotype to IPTG (Fig. 2*E*) and was moderately superinduced in the presence of higher concentrations of D-fucose (*SI Appendix*, Fig. S7). Given the performance of the ${}_{S}I^{+}{}_{YQR}$ BANDPASS, we posited that the ${}_{S}I^{A(2)}{}_{YQR}$ antirepressor also could be antagonized by IPTG post anti-induction, resulting in an antithetical (${}_{S}I^{A(2)}{}_{YQR}$ BANDSTOP) signal processing filter. To test this assertion, first we evaluated the dose–response of the ${}_{S}I^{A(2)}{}_{YQR}$ antirepressor to IPTG (Fig. 2*F*). Congruent with our previous results for transcriptional antirepressors, the ${}_{S}I^{A(2)}{}_{YQR}$ antirepressor objectively performed as a LOWPASS filter—with a PASSBAND between 0 and 0.1 mM IPTG and a STOPBAND > 0.5 mM IPTG. Next, we challenged the ${}_{S}I^{A(2)}$ STOPBAND (i.e., at a fixed IPTG concentration of 1.0 mM) with the noncognate ligand D-fucose to test for mitigation of the response to IPTG (Fig. 2*G*). Namely, we challenged the anti-induced ${}_{S}I^{A(2)}{}_{YQR} \mid O^{SYM}$ unit operation with D-fucose ranging from 0 to 100 mM. Objectively, this unit operation performed as a BANDSTOP signal processing filter—recovering 90% of the original signal at 100 mM D-fucose. This was in contrast to our engineered anti-LacIs (29), which had no apparent mitigation of anti-induction when challenged with D-fucose (*SI Appendix*, Fig. S6). Finally, we constructed a landscape for the ${}_{S}I^{A(2)}{}_{YQR} \mid O^{SYM}$ BANDSTOP signal processing filter to determine if the system had the capacity to vary the center of the BANDWIDTH (Fig. 2*H*). Qualitatively, the ${}_{S}I^{A(2)}{}_{YQR} \mid O^{SYM}$ BANDSTOP unit operation performed similarly to the engineered ${S^{A}}_{YQR}$ BANDSTOP signal processing filter (Fig. 1*H*)—however, with an inverted signal response. Similar performance was observed when the ${}_{S}I^{A(2)}{}_{YQR}$ TF was paired with a native nonsymmetric operator-promoter, forming the ${}_{S}I^{A(2)}{}_{YQR} \mid O^{1}$ unit operation (*SI Appendix*, Fig. S7*E*).

Signal Processing Filters with Alternate DNA Binding—${S^{+}}_{ADR}$ BANDPASS and ${S^{A}}_{ADR}$ BANDSTOP. In an effort to expand the number of nonsynonymous (independent) promoters that can be regulated via biological signal processing filters, we adapted all four TFs used in this study—${S^{+}}_{YQR}$, ${S^{A}}_{YQR}$, ${}_{S}I^{+}{}_{YQR}$, and ${}_{S}I^{A(2)}{}_{YQR}$—with ADR functions and paired each ADR TF with a cognate operator DNA element. Each alternate DNA operator was intercalated between the −35 and −10 hexamers upstream of a reading frame coding for the production of GFP—thus constituting a unique inducible promoter. In total, we constructed six putative promoters, not including $YQR \mid O^{1/SYM}$ (SI Appendix, Table S1). We posited that a given TF adapted with ADR would retain its qualitative signal processing function—though directed to a distinct orthogonal promoter via the operator element. At the outset, we adapted S^{+} and the engineered S^{A} RCDs with ADR to determine if this set of complementary primary topologies could support interactions with complementary DNA operators and respond to the cognate ligand D-fucose (Fig. 3). All six ${S^{+}}_{ADR}$ variants (i.e., ADR = NAR, HQN, TAN, GKR, HTK, and KSL) interacted with cognate DNA operators and were induced by 10 mM D-fucose (Fig. 3*A*). Notably, the ${S^{+}}_{ADR}$ variants displayed differences in dynamic range upon induction and sensitivity to ligand (e.g., half maximal effective concentration = EC_{50}) (*SI Appendix*, Fig. S8). Next, we evaluated this set of ${S^{+}}_{ADR}$ variants response to the noncognate ligand IPTG (Fig. 3*B*). Consistent with our assessment of ${S^{+}}_{YQR}$ (*SI Appendix*, Fig. S1*B*), none of the variants displayed responsiveness to 10 mM IPTG. In turn, we evaluated each of the ${S^{+}}_{ADR}$ variants at 10 mM D-fucose (i.e., ON state) followed by the addition of 10 mM IPTG to determine if any of the variants performed as BANDPASS filters—akin to ${S^{+}}_{YQR}$ (Fig. 3*C*). In all cases, the ${S^{+}}_{ADR}$ variants were antagonized by 10 mM IPTG, reverting each TF back to the OFF state (i.e., all ${S^{+}}_{ADR}$ variants performed as BANDPASS signal processing filters relative to the cognate DNA operator). Next, we evaluated the ${S^{A}}_{ADR}$ variants adapted with alternate DNA binding function (i.e., ADR = NAR, HQN, TAN, GKR, HTK, and KSL) to determine if this collection of engineered unit operations displayed BANDSTOP signal processing functionality. Akin to the ${S^{A}}_{YQR}$ parent TF, all six ${S^{A}}_{ADR}$ variants were anti-induced by 10 mM D-fucose—though resulting in different dynamic ranges (Fig. 3*D* and *SI Appendix*, Fig. S8). Congruent with the ${S^{A}}_{YQR}$ parent, five out of the six ${S^{A}}_{ADR}$ variants performed neutrally to 10 mM IPTG (Fig. 3*E*). Specifically, the ${S^{A}}_{NAR}$ variant was moderately anti-induced by 10 mM IPTG. Finally, we evaluated each of the ${S^{A}}_{ADR}$ variants anti-induced by 10 mM D-fucose (i.e., conferring the OFF state), followed by the addition of 10 mM IPTG (Fig. 3*F*). Briefly, all variants were antagonized by IPTG and resulted in the reversion of each of the ${S^{A}}_{ADR}$ variants back to an apparent ON state (i.e., illustrating coarse-grained BANDSTOP signal processing filter phenotypes). Notably, BANDPASS and BANDSTOP unit operations adapted with alternate DNA binding functions resulted in different PASSBAND or STOPBAND heights, respectively, illustrating another tunable parameter for this collection of biotic regulatory devices (*SI Appendix*, Supplementary Note S4).

Signal Processing Filters with Alternate DNA Binding—${}_{S}I^{+}{}_{ADR}$ BANDPASS and ${}_{S}I^{A(2)}{}_{ADR}$ BANDSTOP. In addition to the S^{+} and S^{A} TFs, we also adapted the engineered ${}_{S}I^{+}$ and ${}_{S}I^{A(2)}$ TFs with alternate DNA binding. We posited (as with previous systems) that ${}_{S}I^{+}$ and ${}_{S}I^{A(2)}$ TFs adapted with alternate DNA binding would retain BANDPASS and BANDSTOP functionality, respectively. In the case of the ${}_{S}I^{+}$ variant, five out of six alternate DNA binding functions resulted in induction with 2.5 mM IPTG—with the exception being ${}_{S}I^{+}{}_{NAR}$ (Fig. 4*A*). Likewise, all ${}_{S}I^{+}{}_{ADR}$ variants (except ${}_{S}I^{+}{}_{NAR}$) were antagonized by 100 mM D-fucose (Fig. 4*C*). None of the ${}_{S}I^{+}{}_{ADR}$ variants were responsive to D-fucose alone (Fig. 4*B*). Next, we constructed and tested ${}_{S}I^{A(2)}{}_{ADR}$ TFs for responsiveness to 2.5 mM IPTG (Fig. 4*D*). As anticipated, all of the ${}_{S}I^{A}{}_{ADR}$ variants were anti-induced by IPTG and were not responsive to D-fucose at the same concentration (Fig. 4*E*). Interestingly, only five out of the six ${}_{S}I^{A(2)}{}_{ADR}$ variants were antagonized by 100 mM D-fucose (with the exception being ${}_{S}I^{A(2)}{}_{NAR}$) (Fig. 4*F*). Together, these results are congruent with our hypothesis that the GalS scaffold has the capacity to support modular adaptation of the DNA binding domain, and the variation in the DNA binding domain required compatibility with a particular allosteric route—evidenced by the variation in dynamic range and lack of functionality when certain engineered regulatory cores were paired with certain alternate DNA binding domains (e.g., ${}_{S}I^{+}{}_{NAR}$ and ${}_{S}I^{A(2)}{}_{NAR}$).

Two-INPUT LOWPASS Filters: Compressed (Integrated) NOR Gates. In total, we identified four variants that were responsive to IPTG. Two variants were antagonized by D-fucose [i.e., 1) the ${}_{S}I^{+}{}_{YQR}$ BANDPASS filter and 2) the ${}_{S}I^{A(2)}{}_{YQR}$ BANDSTOP filter (Fig. 2)] discussed in the previous sections (i.e., *Engineering a Signal Inverted BANDPASS Processing Filter* and *Engineering a Signal Inverted BANDSTOP Processing Filter*). The last two variants were responsive to both ligands (IPTG and D-fucose), and in each case, both ligands resulted in anti-induction (i.e., ${}_{S}I^{A(1)}{}_{YQR}$ and ${}_{S}I^{A(3)}{}_{YQR}$). In turn, we evaluated each antirepressor for responsiveness to IPTG relative to D-fucose to determine the independent performance of each

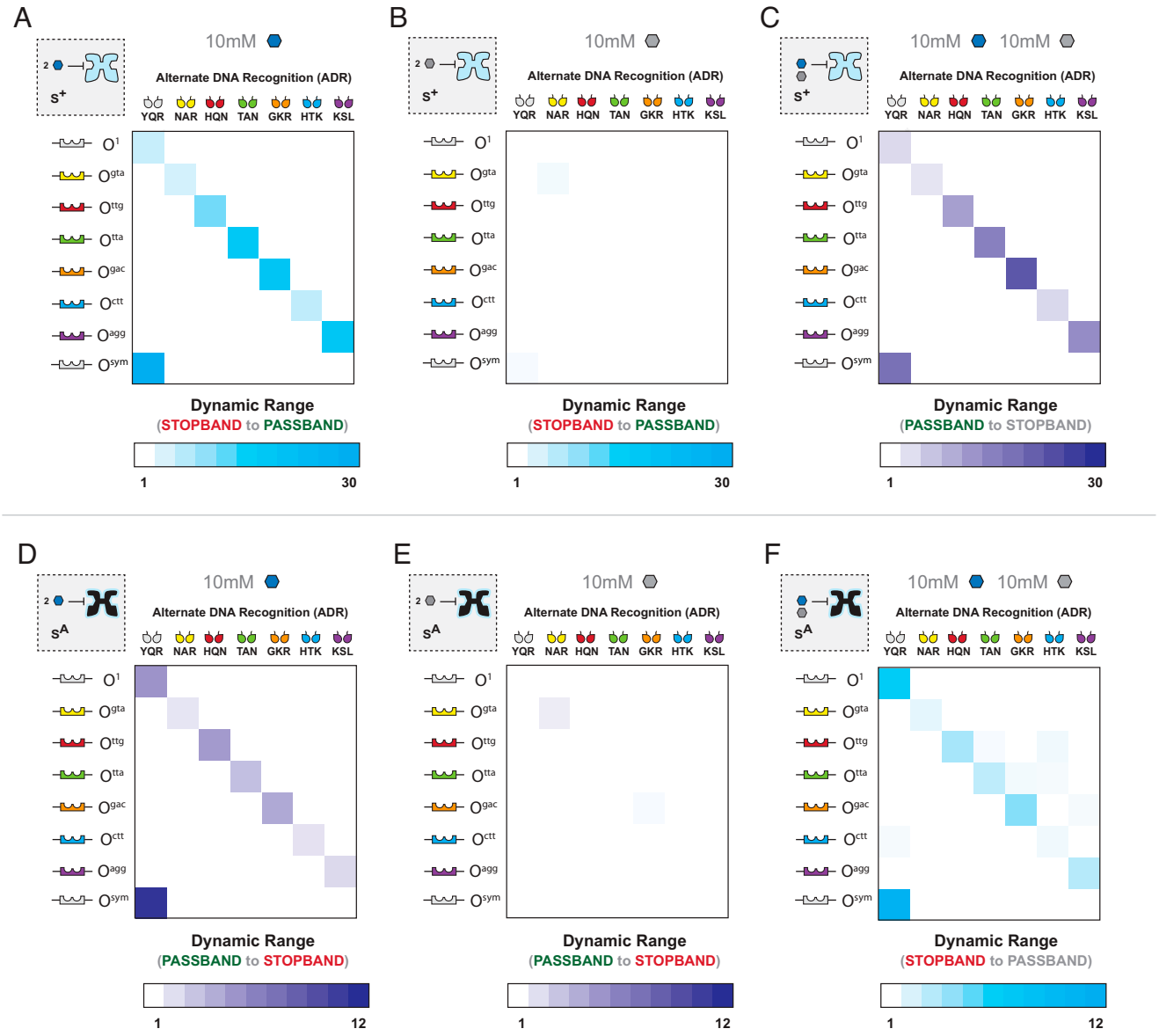

Fig. 3. (*A–C*) BANDPASS and (*D–F*) BANDSTOP matrices for engineered S^{+} and S^{A} protein variants. In matrices, each square represents an operator-DNA binding domain pairing, with DBDs across the *Top* of each matrix and corresponding operators along the *Left*-hand side. For each square, dynamic range is shown as shading relative to the scalebar shown *Below* each matrix. Dynamic ranges were calculated based upon the mean fluorescence (OD_{600} normalized) from $n = 6$ biological replicates for condition state compared to another. Blue signifies induction (fold change increase), whereas purple signifies anti-induction (fold change decrease). (*A*) S^{+}_{ADR} with 10 mM D-fucose. (*B*) S^{+}_{ADR} with 10 mM IPTG. (*C*) S^{+}_{ADR} with 10 mM D-fucose and 10 mM IPTG. (*D*) S^{A}_{ADR} with 10 mM D-fucose. (*E*) S^{A}_{ADR} with 10 mM IPTG. (*F*) S^{A}_{ADR} with 10 mM D-fucose and 10 mM IPTG.

ligand as a single INPUT. Starting with ${}_{S}I^{A(1)}{}_{YQR}$, we performed single-INPUT dose–response curves using IPTG and D-fucose (*SI Appendix*, Fig. S9 *A–D*). Both ligands conferred PASSBAND at low-INPUT concentrations and STOPBAND at high-ligand concentrations (i.e., objectively representing LOWPASS filters in both cases). However, the dynamic range was different for each ligand; namely, IPTG resulted in a larger dynamic range relative to D-fucose for the ${}_{S}I^{A(1)}{}_{YQR}$ variant. Accordingly, we assigned the ${}_{S}I^{A(1)}{}_{YQR}$ unit operation with IPTG as the major LOWPASS filter (*SI Appendix*, Fig. S9*E*) and the ${}_{S}I^{A(1)}{}_{YQR}$ unit operation with D-fucose system as the minor LOWPASS filter (*SI Appendix*, Fig. S9*F*). In the second unit operation, the ${}_{S}I^{A(3)}{}_{YQR}$ TF resulted in an inverted dynamic range in which the D-fucose presented as the major LOWPASS filter (*SI Appendix*, Fig. S9*H*), and IPTG presented as the minor LOWPASS filter (*SI Appendix*, Fig. S9*I*). Moreover, ${}_{S}I^{A(1)}{}_{YQR}$ and ${}_{S}I^{A(3)}{}_{YQR}$ variants were more sensitive to IPTG and thus required a lower concentration of IPTG for anti-induction relative to D-fucose.

Next, we evaluated ${}_{S}I^{A(1)}{}_{YQR} \mid O^{SYM}$ and ${}_{S}I^{A(3)}{}_{YQR} \mid O^{SYM}$ unit operations as a function of two INPUTs (*SI Appendix*, Fig. S9 *G* and *J*). In both cases, we observed moderate variable PASSBAND ranges with respect to the major LOWPASS filter upon the increase in concentration in the minor ligand, respectively. Objectively, ${}_{S}I^{A(1)}{}_{YQR}$ and ${}_{S}I^{A(3)}{}_{YQR}$ can be regarded as compressed NOR logic gates [i.e., NOR gates composed of one TF opposed to two nonsynonymous antirepressors as we previously reported (13)]. Finally, as with the aforementioned engineered TFs, we adapted ${}_{S}I^{A(1)}{}_{ADR}$ and ${}_{S}I^{A(3)}{}_{ADR}$ with alternate DNA binding domains (*SI Appendix*, Fig. S9). The ${}_{S}I^{A(1)}{}_{ADR}$

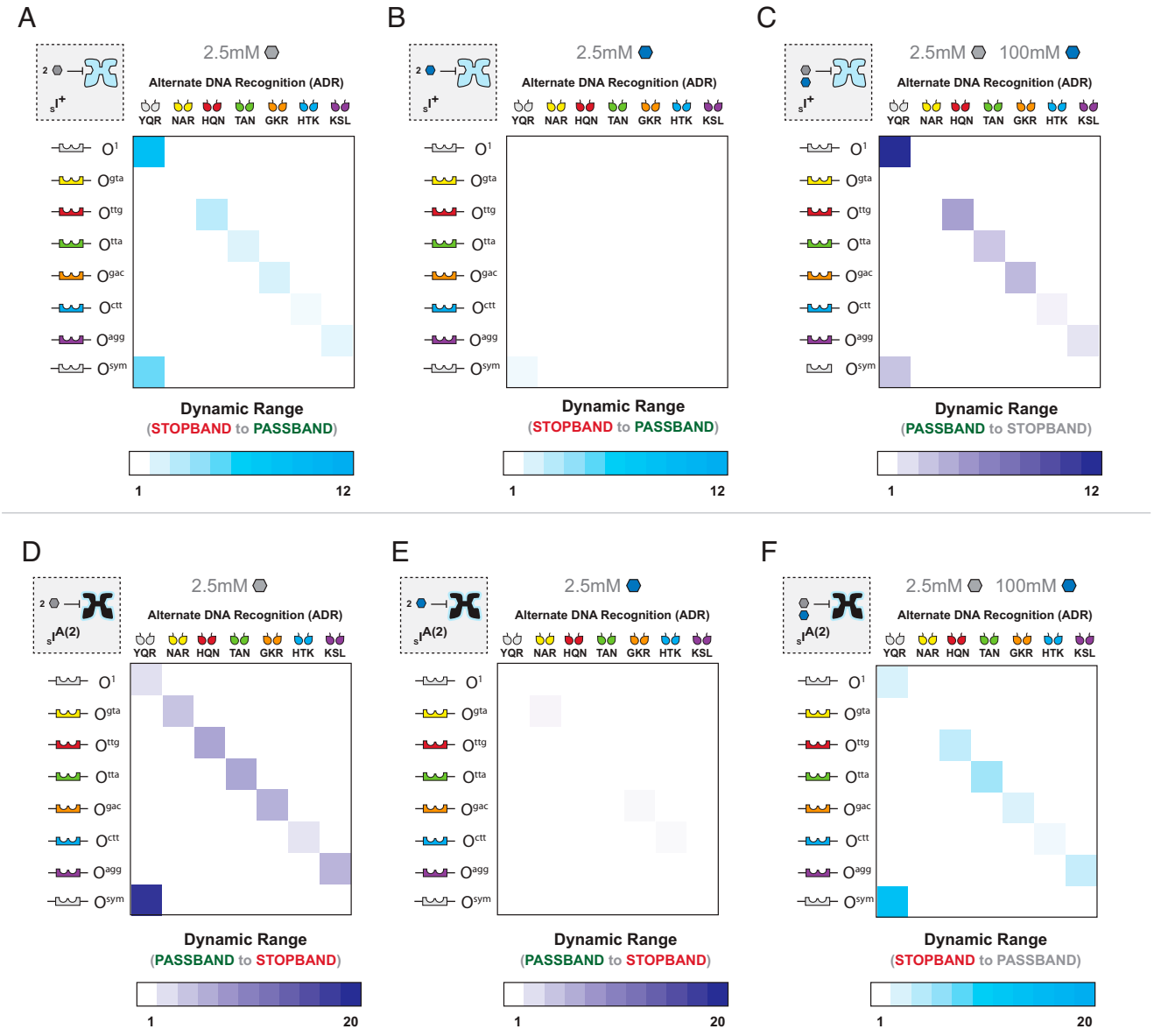

Fig. 4. (*A–C*) BANDPASS and (*D–F*) BANDSTOP matrices for engineered ${}_{S}I^{+}$ and ${}_{S}I^{A(2)}$ protein variants. In matrices, each square represents an operator-DNA binding domain pairing, with DBDs across the *Top* of each matrix and corresponding operators along the *Left*-hand side. For each square, dynamic range is shown as shading relative to the scalebar shown *Below* each matrix. Dynamic ranges were calculated based upon the mean fluorescence (OD_{600} normalized) from $n = 6$ biological replicates for condition state compared to another. Blue signifies induction (fold change increase), whereas purple signifies anti-induction (fold change decrease). (*A*) ${}_{S}I^{+}{}_{ADR}$ with 2.5 mM IPTG. (*B*) ${}_{S}I^{+}{}_{ADR}$ with 2.5 mM D-fucose. (*C*) ${}_{S}I^{+}{}_{ADR}$ with 2.5 mM IPTG and 100 mM D-fucose. (*D*) ${}_{S}I^{A(2)}$ with 2.5 mM IPTG. (*E*) ${}_{S}I^{A(2)}$ with 2.5 mM D-fucose. (*F*) ${}_{S}I^{A(2)}$ with 2.5 mM IPTG and 100 mM D-fucose.

RCD was amenable to ADR adaptation, except ${}_{S}I^{A(1)}{}_{NAR}$, whereas the ${}_{S}I^{A(3)}{}_{ADR}$ variants were functional with all ADR modules. In both cases, ${}_{S}I^{A(1)}{}_{ADR}$ and ${}_{S}I^{A(3)}{}_{ADR}$ variants displayed differences in dynamic range—congruent with previous observations. In general, ${}_{S}I^{A(1)}{}_{ADR}$ variants displayed larger dynamic ranges in response to IPTG—relative to D-fucose at the same concentration. In contrast, ${}_{S}I^{A(3)}{}_{ADR}$ variants displayed larger dynamic ranges in response to D-fucose.

Signal Processing Filter Kinetics. We posited that each of the signal processing filters reported in this study could rapidly transition between regulatory states (e.g., BANDPASS: OFF–ON–OFF) through repeated addition of ligands—based on our proposed mechanism. To test this assertion, we evaluated the kinetics of 1) induction (D-fucose) and induction-mitigation (IPTG) using the ${S^{+}}_{YQR} \mid O^{SYM}$ unit operation and 2) anti-induction (D-fucose) and anti–induction-mitigation (IPTG) via the ${S^{A}}_{YQR} \mid O^{SYM}$ unit operation (Fig. 5). First, we evaluated the kinetics of the ${S^{+}}_{YQR}$ BANDPASS signal processing filter when regulating the production of GFP—such that the performance boundary was defined as the exponential growth region (~4 to 16 h under the conditions tested; *SI Appendix*, Fig. S11), a proxy for continuous growth conditions observed in a bioreactor. In control experiments without ligand (and with the neutral ligand IPTG), no appreciable GFP OUTPUT was observed over a 24-h time course (Fig. 5*A*). In contrast, the addition of D-fucose resulted in a marked increase in GFP OUTPUT with an apparent asymptote observed >16 h—defining the OFF–ON transition (i.e., STOPBAND to PASSBAND). Full BANDPASS functionality was observed via the ${S^{+}}_{YQR} \mid O^{SYM}$ unit operation

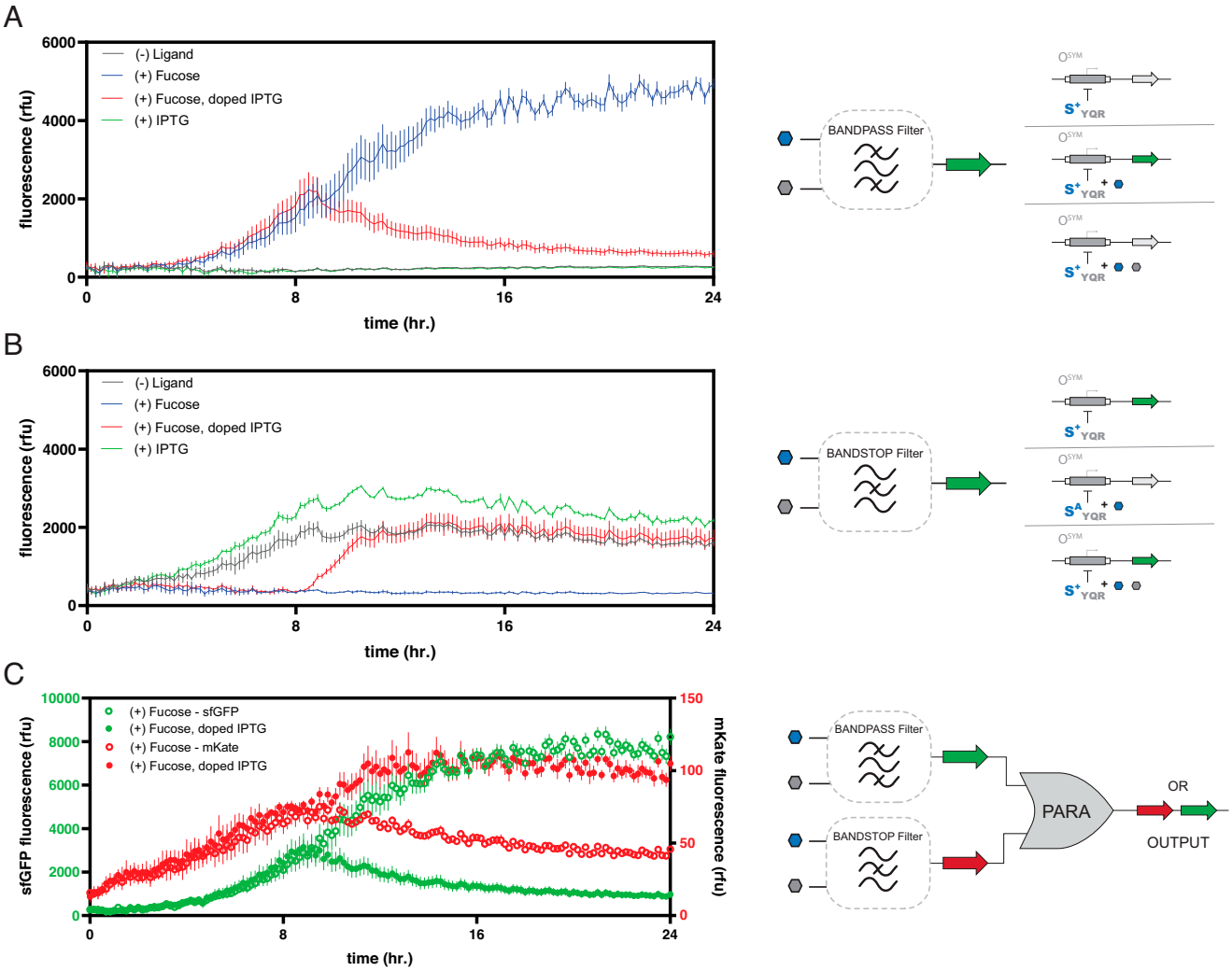

Fig. 5. Dynamic gene regulation by S^{+}_{YQR} and S^{A}_{YQR}. (*A* and *B*) Dynamic BANDPASS and BANDSTOP filters. (*A*) S^{+}_{YQR} | O^{SYM} functions as a BANDPASS filter in real time. Addition of D-fucose at t = 0 h (blue and red lines) causes induction of the sfGFP reporter gene. Otherwise, with the addition of either no ligand or IPTG, the gene is repressed (gray and green lines). When IPTG is doped at t = 8 h, induction is mitigated, turning the gene OFF (red line). (*B*) S^{A}_{YQR} | O^{SYM} functions as a BANDSTOP filter in real time. Addition of D-fucose at t = 0 h (blue and red lines) causes anti-induction of the sfGFP reporter gene, keeping the gene OFF. Otherwise, with the addition of either no ligand or IPTG, the gene is constitutively expressed (gray and green lines). When IPTG is doped at t = 8 h, anti-induction is mitigated, turning the gene ON (red line). The induction from IPTG (green line) is higher than that with no ligand (gray line) due to IPTG causing greater than basal levels of expression. Connected points represent means of OD_{600} normalized fluorescence of n = 6 biological replicates, with error bars representing ±1 SD, measured every 10 min as cells grew for 24 h. (*C*) Simultaneous regulation of two genes by open-loop control. In a single cell strain, S^{+}_{TAN} regulates O^{tta}-sfGFP, and S^{A}_{YQR} regulates O^{SYM}-mKate2. Cells were grown over 24 h in either only fucose or fucose doped with IPTG after 8 h. The *Left* axis (green) denotes relative OD_{600} normalized fluorescence of sfGFP, while the *Right* (red) denotes relative fluorescence of mKate2, with points of the same colors showing either the fucose (open circles) or fucose and IPTG (closed circles) conditions. Points shown are the means of n = 6 biological replicates, with error bars representing ±1 SD, measured every 10 min. Addition of IPTG at 8 h is able to invert the regulatory function for each gene: the BANDPASS filter goes from induced (ON) to anti-induced (OFF), while the BANDSTOP filter goes from anti-induced (OFF) to induced (ON).

upon the addition of D-fucose followed by the addition of IPTG at 8 h (induction-mitigation) (Fig. 5*A*). Namely, in this experiment we observed an increase in GFP production up to 8 h and a subsequent and immediate decrease in GFP OUTPUT after the addition of IPTG. Similar BANDPASS performance was observed using a red fluorescent protein (RFP, mKate2) as the OUTPUT (*SI Appendix*, Figs. S10 and S11). Next, we evaluated the kinetics for the engineered S^{A}_{YQR} | O^{SYM} unit operation (Fig. 5*B*). Given that this BANDSTOP signal processing filter starts in the PASSBAND state the control experiment (without ligand) was congruent with the constitutive production of GFP. Likewise, when cultured with neutral ligand (IPTG), a similar kinetic isotherm was observed—though with a slightly higher OUTPUT maxima (*SI Appendix*, Supplementary Note S3). As expected, when the S^{A}_{YQR} | O^{SYM} unit operation was dosed with 10 mM D-fucose, anti-induction occurred and GFP OUTPUT was repressed (Fig. 5*B*). In turn, BANDSTOP signal processing was observed when the S^{A}_{YQR} repressed state (i.e., with 10 mM D-fucose) was dosed with 10 mM IPTG—which resulted in a transition from the anti-induced STOPBAND to the PASSBAND state (Fig. 5*B*). Similar BANDSTOP performance was observed using the RFP (mKate2) as the OUTPUT (*SI Appendix*, Fig. S10 *C–F*).

Signal Processing Filter Programming—Open Loop Control System. Next, we evaluated the in tandem (signal-coupled) performance

of a BANDPASS unit-operation regulating GFP (green-channel, sfGFP) and a BANDSTOP unit-operation regulating RFP (red-channel, mKate2)—in parallel in a single chassis cell (Fig. 5*C*). Namely, to direct each TF to different promoters in the same chassis cell, we used $S^{+}{}_{TAN}$ and $S^{A}{}_{YQR}$, which were adapted with disparate DNA binding domains that orthogonally directed each TF to O^{tta} (green-channel) and O^{SYM} (red-channel) promoter-operators, respectively. Given that the cognate ligand is D-fucose for both TFs ($S^{+}{}_{TAN}$ and $S^{A}{}_{YQR}$), the resulting circuit can be regarded as signal-coupled though phenotypically opposite. To demonstrate the function of this signal-coupled circuit, we started with unit-operations exposed to the cognate ligand D-fucose, and at 8 h, this set of unit operations was doped with IPTG to mitigate induction (green-channel), or to mitigate anti-induction (red-channel). As shown in Fig. 5*C*, a marked switch in OUTPUT can be observed, where upon the addition of IPTG the green-channel transitions from the induced PASSBAND (ON) to the STOPBAND (OFF) and concurrently the red-channel transitions from the anti-induced STOPBAND (OFF) to the PASSBAND (ON) (Fig. 5*C*). The depicted in tandem kinetic BANDPASS and BANDSTOP device is not inherently limited by one transition. Given that the user starts with low concentrations of INPUT ligands repeated addition of ligand can potentially allow for additional cycles. Similar dynamic signal-coupled OUTPUT switching was observed using the ${}_{S}I^{A(2)}{}_{YQR}$ BANDSTOP (green-channel) and ${}_{S}I^{+}{}_{TAN}$ BANDPASS (red-channel) unit operations—though signal inverted (*SI Appendix*, Fig. S10).

Discussion

Deconvolution of the mutations that resulted in this collection of engineered TFs can help shed light on the extent of plasticity for conferring 1) alternate allosteric communication and 2) alternate ligand binding in the GalS topology. Namely, the process for conferring alternate allosteric communication in $S^{A}{}_{YQR}$ and ${}_{S}I^{+}{}_{YQR}$ engineered TFs required a block in allosteric communication at position 95—resulting in insensitivity to both IPTG and D-fucose (*SI Appendix*, Fig. S3). Evidently, compensatory mutations were required to confer the reported phenotypes for both variants (*SI Appendix*, Fig. S12). In both variants, no changes to the binding pocket occurred—thus, we posited that the observed phenotypes for $S^{A}{}_{YQR}$ and ${}_{S}I^{+}{}_{YQR}$ were achieved by alternate allosteric communication alone. Of significant note in the ${}_{S}I^{+}{}_{YQR}$ variant, the compensatory mutation (S72T) conferred alternate ligand specificity—without altering the binding pocket. This result is in contrast to contemporary protein–ligand design rules that prioritize the role of the constellation of amino acid sidechains that are in direct contact with the ligand to achieve alternate ligand binding. Clearly, the role of residues in proximity to the ligand can be important for conferring alternate ligand binding in the GalS topology—evidenced by variants ${}_{S}I^{A(1)}{}_{YQR}$ and ${}_{S}I^{A(3)}{}_{YQR}$ in which modifications to the effector binding pocket were required to achieve alternate ligand binding (*SI Appendix*, Figs. S3 and S4). However, the former observations for the $S^{A}{}_{YQR}$ and ${}_{S}I^{+}{}_{YQR}$ variants introduces a more granular design option and highlights the importance of considering the allosteric route when designing novel ligand binding in functional proteins. This observation is reinforced in the ${}_{S}I^{A(2)}{}_{YQR}$ variant, which was devoid of a block in allosteric communication at position 95. However, the ${}_{S}I^{A(2)}{}_{YQR}$ variant utilized an alternate block in allosteric communication to IPTG at position 324 (*SI Appendix*, Fig. S12). Likewise, none of the compensatory mutations resulted in changes to the effector binding pocket. Accordingly, this observation was consistent with our general hypothesis for conferring alternate allosteric communication. Notably, adaptation of all the TFs in this study with alternate DNA binding preserved the qualitative function of each of the unit operations. However, the dynamic range in nearly every system was affected. Collectively, this highlights a set of coarse-grained design rules for engineering de novo TFs in the broader LacI/GalR topology [i.e., engineers need to consider and couple 1) the allosteric route, 2) to a particular ligand binding pocket, and 3) pair the aforementioned with physicochemical properties of the protein–DNA interaction].

In addition to improving our understanding of allosteric communication and TF protein design rules, the BANDPASS and BANDSTOP signal processing filters developed in this study have the potential to significantly improve bioreactor dynamics because they involve repeated addition, rather than addition and removal, of small molecules to alter regulatory phenotype and function. The concentration changes required to completely desorb a signal molecule are much higher than those to adsorb a new molecule due to the typical values of dissociation constants in these protein–molecule complexes. For instance, bioreactor time constants and spatial variations in concentrations can be significant barriers to consistent performance, and the biological filters developed in this study can reduce these barriers due to requiring smaller changes to affect performance and combatting stochastic noise variation in INPUT to achieve an OUTPUT (46). Moreover, given the structure of the genetic architecture (i.e., the DNA operator intercalated between the −35 and −10 promoter hexamers), the emerging technology also contributes to improving resource partitioning (44). Namely, by directing a given TF to the binding region for RNAP, the corresponding device maximizes the free state of RNAP upon binding of the TF, thus resulting in a more efficient synthetic biology part and reducing one aspect of metabolic burden.

Methods

Strains, Plasmids, and Media. All assay experiments were performed in the *E. coli* strain 3.32 (*lacZ13(Oc) lacI22 λ- el4- relA1 spoT thiE1*; Yale Coli Genetic Stock Center No. 5237), transformed chemically, while DNA cloning was performed in New England Biolabs 5-alpha Competent *E. coli* (*huA2 Δ*(argF-lacZ)U169 phoA glnV44 φ80Δ(lacZ)M15 gyrA96 recA1 relA1 endA1 thi-1 hsdR17; New England Biolabs). Cells were grown in Luria Broth (LB) Miller Medium (Fisher Scientific) or M9 Minimal Medium (6.8 g · L^{-1} Na_2HPO_4, 3.0 g · L^{-1} KH_2PO_4, 0.5 g · L^{-1} NaCl, 1.0 g · L^{-1} NH_4Cl, 2 mM $MgSO_4$, 100 μM $CaCl_2$; Millipore Sigma) supplemented with 0.2% (wt/vol) casamino acids (VWR Life Sciences), 1 mM thiamine HCl (Alfa Aesar), and 100 mM glucose (Fisher Scientific). LB Miller Agar (Fisher Scientific) was used for selection when cloning. Antibiotics and ligands were used as appropriate. Antibiotics used were the following: chloramphenicol (25 μg · mL^{-1}; VWR Life Sciences) and kanamycin (35 μg · mL^{-1}; VWR Life Sciences); ligands used were the following: isopropyl-β-D-1-thiogalactoside (IPTG; GoldBio) and D-fucose (Carbosynth). All ligands were prepared in a dilution series from a stock concentration, then added to media.

Protein Mutagenesis and Library Creation. All site-directed mutagenesis was performed using inverse PCR, while site-saturation mutagenesis was performed similarly, using inverse PCR with NNS degenerate primers. Following treatment with KLD enzyme mix (KLD = T4 Polynucleotide Kinase, Salt T4 Ligase, and DpnI; New England Biolabs), the DNA product was transformed into NEB 5-alpha Competent Cells (New England Biolabs), then selected for on plates grown overnight at 37 °C. For single site-directed mutagenesis, single colonies were picked, and plasmids were isolated to confirm sequence; for protein libraries, colonies were streaked from plates or were transformed directly into liquid flasks (for the error-prone library), then plasmids were isolated. The error-prone library was generated using the protocol detailed by Groseclose et al. (13). Briefly, in one PCR, the $pGalS_{YQR}$ vector was linearized excluding the region corresponding to the RCD (residues 62 to 348). In a second PCR, the $GalS_{YQR}$ RCD was subjected to EP-PCR. A master library with 5- to 7-base pair (bp) (3- to 5-residue) mutations, on average, over the 864-bp amplicon (~0.8% error frequency) was constructed in a reaction with 1.25 U Taq DNA Polymerase (New England Biolabs), 1× Taq Mg-free Buffer, 1.8 mM $MgCl_2$ (Millipore Sigma), 200 μM $MnCl_2$ (Millipore Sigma), 400 μM dCTP (New England Biolabs), 400 μM dTTP (New England Biolabs), 80 μM dGTP (New

England Biolabs), 80 μM dATP (New England Biolabs), 500 μM, each, forward and reverse primers, and 10 ng (4.2 fmol) $pGalS_{YQR}$ plasmid as the template. The reaction was subjected to 95 °C for 3 min and 20 cycles of 95 °C for 30 s, followed by 68 °C for 5 min, and a final extension at 68 °C for 10 min. The vector and error-prone RCD insert were both visualized on gels and the vector was then PCR cleaned up (Qiagen), while the insert was gel extracted (Qiagen), then reamplified by PCR and finally PCR cleaned up (Qiagen). The two fragments were then combined via circular polymerase extension cloning, then transformed into electrocompetent 5-alpha *E. coli* cells. The library size was estimated to be on the order of 10^8 colony forming units. Following plasmid isolation, libraries for screening were developed by performing site-directed mutagenesis on the master library to introduce discovered superrepressor mutations.

Cell Sorting and Screening. Cultures were prepared similarly to those for the microplate assay and as done by Richards et al. (29). Briefly, colonies were inoculated in LB with relevant antibiotics (chloramphenicol for pLacI, kanamycin for the GFP reporter) and grown overnight at 37 °C, shaking at 300 rpm. Cultures were then diluted 1:100 in supplemented M9 Minimal Media containing relevant antibiotics and ligands, as called for, in sterile culture tubes (Nunc) and grown at 37 °C, shaking at 300 rpm, for 20 h. Each culture was then aliquoted such that the optical density (OD600) would be approximately equal to 0.2 (WPA Biowave CO8000 Cell Density Meter) in the final solution volume (typically 1 mL). Cells were then pelleted at 14,000 rpm for 2 min. The supernatant was then discarded, and cells were resuspended in phosphate-buffered saline (PBS) supplemented with 25 mM Hepes (Fisher Scientific), 1 mM ethylenediaminetetraacetic acid (EDTA) (Millipore Sigma), and 0.01% (vol/vol) Tween20 (VWR Life Sciences), and again pelleted at 14,000 rpm for 3 min. This wash step was repeated once before cells were finally resuspended in PBS supplemented with 25 mM Hepes and 1 mM EDTA. When appropriate, ligand concentrations in cell sorting were 10 mM. Cytometry experiments were performed using a BD FACSAria Fusion flow cytometer (BD Biosciences) equipped with a 100-mW 488-nm laser for excitation, a 510/30-nm bandpass emission filter, and an 85-μm nozzle. Cells were interrogated measuring fluorescein isothiocyanate-Area (FITC-A) at flow rates between 10 and 30 $\mu L \cdot min^{-1}$. Events were gated on forward- and side-scatter, and a threshold was set by side-scatter (5,000), with doublets discriminated against using standard forward scatter-Area versus -Height and side scatter-Area versus -Height plots. During sorts, 50,000 to 100,000 events were collected, sorted directly into LB (with antibiotic), then cultured overnight at 37 °C, shaking at 300 rpm, in culture tubes (Nunc). This culture was then used to inoculate for another day of sorting after being prepared, as in the current section *Cell Sorting and Screening*.

Sorts for S^A phenotype consisted of two sequential sort steps: the first with the ligand (D-fucose), collecting the low-fluorescence mutants (S^S and S^A, screening out residual wild-type S^+ and nonfunctional S^-), the second without ligand, collecting the high-fluorescence mutants (discriminating between S^S and S^A). Sorts for the $_sI^+$ and $_sI^A$ phenotypes consisted of similar sequential steps, with the first collecting the low-fluorescence mutants (no ligand, IPTG, for $_sI^+$, and with ligand for the $_sI^A$ phenotype), and the second collecting the high-fluorescence mutants (with ligand, IPTG, for $_sI^+$, and without ligand for the $_sI^A$ phenotype). Low-fluorescence collection was always selected as the first sort step to screen out the abundance of nonfunctional (likely misfolded) mutants. Gates for low and high fluorescence were determined from controls with known cytometry performance [i.e., Lac_{NULL}, parent S^S, and I^A and I^S variants from Richards et al. (29)]. For the settings utilized, the high-fluorescence mutants were binned $\geq 1 \times 10^5$ FITC-A, while low-fluorescence mutants binned $<1 \times 10^5$ FITC-A. Each individual sort step was repeated once to enrich the desired population and filter out false positives. Sorting was performed using the BD FACSDiva (BD Biosciences) software package. Following the final sorts, cells were grown overnight at 37 °C, shaking at 300 rpm in LB with antibiotics, then plated on selection plates. Once grown overnight at 37 °C, individual colonies were screened via the microplate assay to verify phenotype and determine performance characteristics. Up to 480 colonies were picked to be screened via microwell plate to verify phenotype; however, sequencing confirmed verified mutants were always found within the first 96 colonies screened.

Time-Course Experiments. This protocol was adapted from the microwell plate protocol (*SI Appendix, Supplementary Methods*). Briefly, colonies were inoculated in LB with relevant antibiotics (chloramphenicol for pLac, kanamycin for the reporter) and grown overnight at 37 °C, shaking at 300 rpm. Cultures were then diluted 1:200 in 200 μL supplemented M9 Minimal Media containing relevant antibiotics and ligands, as called for, in the wells of a 96-well, sterile, flat- and clear-bottomed, black-sided microwell plate (Greiner). All assay trials (consisting of a TF variant with inducers) were measured in biological replicates of $n = 6$. Clear lids were placed on microplates, which were then grown at 37 °C for 24 h in a plate reader (Molecular Devices SpectraMax M2e). Fluorescence (sfGFP—excitation: 485 nm, emission: 510 nm; mKate2—excitation: 588 nm, emission: 635 nm) intensity and OD_{600} were measured every 10 min., with shaking for 1 min preceding each read. When appropriate, ligands were doped after 8 h of growth, 1:200 volume from concentrated stock. For the S^+ and S^A variants, IPTG and D-fucose were added at 10 mM each, whereas for the $_sI^+$ and $_sI^{A(2)}$ variants, IPTG was added at 1 mM and D-fucose at 10 mM. Data were collected with SoftMax Pro Software (Molecular Devices). Fluorescence intensity was normalized to cell density and data were analyzed and plotted using Microsoft Excel (Microsoft) and GraphPad (Prism).

Data Availability. Data supporting the findings of this work are available within the paper and its supporting information files (with DNA developed in this paper uploaded 13 and 14 May 2021). The plasmid sequences may be found deposited in GenBank: Reporter Plasmids (MT127263–MT127272), anti-LacI Plasmids (MZ198809–MZ198810 and MN207937), dual-TF Plasmids (MZ198788–MZ198789), pLacI (MT127274), pLacNULL Plasmid (MT127273), GalS Plasmids (MN207929–MN207935), anti-GalS Plasmids (MZ198779–MZ198785), GalS Super-Repressor Plasmids (MZ198790–MZ198794), SIA Plasmids (MZ198818–MZ198824 and MZ198795–MZ198808), SI+ Plasmids (MZ198811–MZ198817), and GFP/mKate Reporter Plasmids (MZ198786–MZ198787). Protein sequences for wild-type LacI and GalS proteins can be found in the UnitProt database with accession numbers: P03023 (LacI) and P25748 (GalS). All other study data are included in the article and/or *SI Appendix*.

ACKNOWLEDGMENTS. This work was supported by NSF Grants MCB 2123855 and GCR 1934836, MCB 1921061, CBET 1844289, CBET 1804639, and MCB 1747439, all awarded to C.J.W.

1. P. E. Purnick, R. Weiss, The second wave of synthetic biology: From modules to systems. *Nat. Rev. Mol. Cell Biol.* **10**, 410–422 (2009).
2. A. S. Khalil, J. J. Collins, Synthetic biology: Applications come of age. *Nat. Rev. Genet.* **11**, 367–379 (2010).
3. A. A. K. Nielsen, T. H. Segall-Shapiro, C. A. Voigt, Advances in genetic circuit design: Novel biochemistries, deep part mining, and precision gene expression. *Curr. Opin. Chem. Biol.* **17**, 878–892 (2013).
4. T. M. Groseclose *et al.*, Biomolecular systems engineering: Unlocking the potential of engineered allostery via the lactose repressor topology. *Annu. Rev. Biophys.* **50**, 303–321 (2021).
5. J. K. Rogers *et al.*, Synthetic biosensors for precise gene control and real-time monitoring of metabolites. *Nucleic Acids Res.* **43**, 7648–7660 (2015).
6. T. S. Gardner, C. R. Cantor, J. J. Collins, Construction of a genetic toggle switch in Escherichia coli. *Nature* **403**, 339–342 (2000).
7. M. Taketani *et al.*, Genetic circuit design automation for the gut resident species Bacteroides thetaiotaomicron. *Nat. Biotechnol.* **38**, 962–969 (2020).
8. S. Slomovic, K. Pardee, J. J. Collins, Synthetic biology devices for in vitro and in vivo diagnostics. *Proc. Natl. Acad. Sci. U.S.A.* **112**, 14429–14435 (2015).
9. D. Del Vecchio, H. Abdallah, Y. Qian, J. J. Collins, A blueprint for a synthetic genetic feedback controller to reprogram cell fate. *Cell Syst.* **4**, 109–120.e11 (2017).
10. A. Milias-Argeitis, M. Rullan, S. K. Aoki, P. Buchmann, M. Khammash, Automated optogenetic feedback control for precise and robust regulation of gene expression and cell growth. *Nat. Commun.* **7**, 12546 (2016).
11. A. A. Nielsen *et al.*, Genetic circuit design automation. *Science* **352**, aac7341 (2016).
12. R. E. Rondon, T. M. Groseclose, A. E. Short, C. J. Wilson, Transcriptional programming using engineered systems of transcription factors and genetic architectures. *Nat. Commun.* **10**, 4784 (2019).
13. T. M. Groseclose, R. E. Rondon, Z. D. Herde, C. A. Aldrete, C. J. Wilson, Engineered systems of inducible anti-repressors for the next generation of biological programming. *Nat. Commun.* **11**, 4440 (2020).
14. J. Bonnet, P. Yin, M. E. Ortiz, P. Subsoontorn, D. Endy, Amplifying genetic logic gates. *Science* **340**, 599–603 (2013).
15. P. Siuti, J. Yazbek, T. K. Lu, Synthetic circuits integrating logic and memory in living cells. *Nat. Biotechnol.* **31**, 448–452 (2013).
16. J. R. Rubens, G. Selvaggio, T. K. Lu, Synthetic mixed-signal computation in living cells. *Nat. Commun.* **7**, 11658 (2016).
17. S. Basu, Y. Gerchman, C. H. Collins, F. H. Arnold, R. Weiss, A synthetic multicellular system for programmed pattern formation. *Nature* **434**, 1130–1134 (2005).
18. F. Meng, T. Ellis, The second decade of synthetic biology: 2010-2020. *Nat. Commun.* **11**, 5174 (2020).
19. M. B. Elowitz, S. Leibler, A synthetic oscillatory network of transcriptional regulators. *Nature* **403**, 335–338 (2000).
20. N. Yosef, A. Regev, Impulse control: Temporal dynamics in gene transcription. *Cell* **144**, 886–896 (2011).

21. L. Swint-Kruse, K. S. Matthews, Allostery in the LacI/GalR family: Variations on a theme. *Curr. Opin. Microbiol.* **12**, 129–137 (2009).
22. Z. D. Herde *et al.*, Engineering allosteric communication. *Curr. Opin. Struct. Biol.* **63**, 115–122 (2020).
23. C. J. Wilson, H. Zhan, L. Swint-Kruse, K. S. Matthews, The lactose repressor system: Paradigms for regulation, allosteric behavior and protein folding. *Cell. Mol. Life Sci.* **64**, 3–16 (2007).
24. D. L. Shis, F. Hussain, S. Meinhardt, L. Swint-Kruse, M. R. Bennett, Modular, multi-input transcriptional logic gating with orthogonal LacI/GalR family chimeras. *ACS Synth. Biol.* **3**, 645–651 (2014).
25. R. E. Rondon, C. J. Wilson, Engineering a new class of anti-LacI transcription factors with alternate DNA recognition. *ACS Synth. Biol.* **8**, 307–317 (2019).
26. C. T. Y. Chan, J. W. Lee, D. E. Cameron, C. J. Bashor, J. J. Collins, 'Deadman' and 'Passcode' microbial kill switches for bacterial containment. *Nat. Chem. Biol.* **12**, 82–86 (2016).
27. F. J. Poelwijk, M. G. J. de Vos, S. J. Tans, Tradeoffs and optimality in the evolution of gene regulation. *Cell* **146**, 462–470 (2011).
28. S. Meyer *et al.*, Engineering alternate cooperative-communications in the lactose repressor protein scaffold. *Protein Eng. Des. Sel.* **26**, 433–443 (2013).
29. D. H. Richards, S. Meyer, C. J. Wilson, Fourteen ways to reroute cooperative communication in the lactose repressor: Engineering regulatory proteins with alternate repressive functions. *ACS Synth. Biol.* **6**, 6–12 (2017).
30. R. Rondon, C. J. Wilson, Engineering alternate ligand recognition in the PurR topology: A system of novel caffeine biosensing transcriptional antirepressors. *ACS Synth. Biol.* **10**, 552–565 (2021).
31. O. Scholz, M. Köstner, M. Reich, S. Gastiger, W. Hillen, Teaching TetR to recognize a new inducer. *J. Mol. Biol.* **329**, 217–227 (2003).
32. J. W. Ellefson, M. P. Ledbetter, A. D. Ellington, Directed evolution of a synthetic phylogeny of programmable Trp repressors. *Nat. Chem. Biol.* **14**, 361–367 (2018).
33. S.-Y. Tang, H. Fazelinia, P. C. Cirino, C. Ara, AraC regulatory protein mutants with altered effector specificity. *J. Am. Chem. Soc.* **130**, 5267–5271 (2008).
34. J. Wu *et al.*, Design and application of a lactulose biosensor. *Sci. Rep.* **7**, 45994 (2017).
35. M. D. Barkley, A. D. Riggs, A. Jobe, S. Burgeois, Interaction of effecting ligands with lac repressor and repressor-operator complex. *Biochemistry* **14**, 1700–1712 (1975).
36. C. J. Wilson, H. Zhan, L. Swint-Kruse, K. S. Matthews, Ligand interactions with lactose repressor protein and the repressor-operator complex: The effects of ionization and oligomerization on binding. *Biophys. Chem.* **126**, 94–105 (2007).
37. M. J. Weickert, S. Adhya, Control of transcription of gal repressor and isorepressor genes in Escherichia coli. *J. Bacteriol.* **175**, 251–258 (1993).
38. M. J. Weickert, S. Adhya, A family of bacterial regulators homologous to Gal and Lac repressors. *J. Biol. Chem.* **267**, 15869–15874 (1992).
39. S. Meinhardt *et al.*, Novel insights from hybrid LacI/GalR proteins: Family-wide functional attributes and biologically significant variation in transcription repression. *Nucleic Acids Res.* **40**, 11139–11154 (2012).
40. G. Buttin, Mécanismes régulateurs dans la biosynthèse des enzymes du métabolisme du galactose chez Escherichia coli K12: I. La biosynthèse induite de la galactokinase et l'induction simultanée de la séquence enzymatique. *J. Mol. Biol.* **7**, 164–182 (1963).
41. T. Sohka *et al.*, An externally tunable bacterial band-pass filter. *Proc. Natl. Acad. Sci. U.S.A.* **106**, 10135–10140 (2009).
42. A. Tamsir, J. J. Tabor, C. A. Voigt, Robust multicellular computing using genetically encoded NOR gates and chemical 'wires'. *Nature* **469**, 212–215 (2011).
43. L. de Mena, P. Rizk, D. E. Rincon-Limas, Bringing light to transcription: The optogenetics repertoire. *Front. Genet.* **9**, 518 (2018).
44. J. A. Davey, C. J. Wilson, Engineered signal-coupled inducible promoters: Measuring the apparent RNA-polymerase resource budget. *Nucleic Acids Res.* **48**, 9995–10012 (2020).
45. N. D. Taylor *et al.*, Engineering an allosteric transcription factor to respond to new ligands. *Nat. Methods* **13**, 177–183 (2016).
46. S. Hooshangi, S. Thiberge, R. Weiss, Ultrasensitivity and noise propagation in a synthetic transcriptional cascade. *Proc. Natl. Acad. Sci. U.S.A.* **102**, 3581–3586 (2005).